Cold sensitivity of the SARS-CoV-2 spike ectodomain

Robert J Edwards[1,2‡,*], Katayoun Mansouri[1,‡], Victoria Stalls[1,‡], Kartik Manne[1, ‡],

Brian Watts[1], Rob Parks[1], Sophie M. C. Gobeil[1], Katarzyna Janowska[1], Dapeng Li[1], Xiaozhi Lu[1],

Margaret Deyton[1], Jordan Sprenz[1], Wilton Williams[1,2], Kevin Saunders[1,3], Gregory D.

Sempowski[1], Rory Henderson[1,2], Munir Alam[1,2], Barton F. Haynes[1,2], Priyamvada Acharya[1,3,*]

Affiliations:
[1] Duke Human Vaccine Institute, Durham NC 27710, USA
[2] Duke University, Department of Medicine, Durham NC 27710, USA
[3] Duke University, Department of Surgery, Durham NC 27710, USA
[4] Duke University, Department of Immunology, Durham NC 27710, USA
‡These authors contributed equally.
*To whom correspondence should be addressed

Correspondence to: Robert J Edwards (rj.edwards@duke.edu) and Priyamvada Acharya (priyamvada.acharya@duke.edu)

Highlights

- SARS-CoV-2 S ectodomain construct, widely used for vaccine studies, exhibits cold sensitivity.
- Negative stain electron microscopy shows disintegration of spike structure upon storage at 4 °C.
- Differential scanning calorimetry measurements confirm destabilization by cold.
- Cold storage alters antigenicity of SARS-CoV-2 spike.
- Brief incubation at 37 °C restored spike integrity after cold-storage.

Summary

The impact of COVID-19 and the urgency to develop a vaccine against the SARS-CoV-2 virus cannot be overstated. The viral fusion spike (S) protein ectodomain is the primary target for vaccine development. Here we report an unexpected cold sensitivity of a stabilized SARS-CoV-2 ectodomain construct currently being widely used for immunogen design. We found that when stored at 22 or 37 °C for 1 week, the S-protein displayed well-ordered trimeric spikes by negative stain electron microscopy. However, storage at 4 °C reduced the trimeric spikes to <10%, accompanied by decreased stability and enhanced exposure of the ACE-2 receptor binding site. Well-formed S particles could be recovered from cold-stored samples by a brief incubation at 37 °C. Our results will have broad impact on structural, functional and vaccine studies using the SARS-CoV-2 S ectodomain.

Introduction

The COVID-19 pandemic has spurred accelerated efforts to develop effective countermeasures to address the ongoing global health emergency. The spike (S) protein of SARS-CoV-2 mediates receptor binding and cell entry and is a key target for vaccine development efforts. This highly dynamic protein exhibits substantial conformational flexibility, transitioning between pre-fusion “down” and “up” states that alter the initial accessibility of the receptor binding domain (RBD), and subsequently transitioning to a post-fusion conformation that mediates fusion of viral and cellular membranes. Stabilized S ectodomain constructs have been developed that present a native-like architecture and mimic the spike ectodomain displayed on the virion (*1*). These constructs are capable of binding to the ACE-2 receptor (*2, 3*), present epitopes for neutralizing antibodies on their surface (*4-6*), and have facilitated structural, biochemical and biophysical studies on the S protein, its interactions with the immune system, and the mechanism of S-mediated cellular entry and immune evasion. Here we report on the cold sensitivity of SARS-CoV-2 S protein ectodomain constructs.

Results and Discussion

The SARS-CoV-2 construct discussed here incorporates residues 1-1208, and harbors two stabilizing proline mutations in the S2 domain, a foldon trimerization domain, and C-terminal Twin Streptactin and Histidine (His) tags (Figure 1A). Similar constructs are currently being widely used for structural biology and vaccine studies (*2-4, 7, 8*). Proteins are expressed in HEK-293F cells and purified via a Streptactin column and size exclusion chromatography (SEC) (*9*). Initial sample assessment is by SDS-PAGE, SEC, differential scanning fluorimetry (DSF) (*10*), and negative stain electron microscopy (NSEM). NSEM proved to be especially important because it reveals the three-dimensional integrity of individual molecules, allowing us to discriminate between preparations that otherwise looked similar by bulk measures such as SDS-PAGE and SEC (Figure 1B and C). We also used automatic particle picking and 2D class

averaging to quantify the fraction of intact spike. Good preparations showed a high fraction of kite-shaped particles (Figure 1B, inset) as would be expected when the trimeric spike structure (*2, 9, 11, 12*) lies flat on the carbon film; whereas some preparations showed fewer spike particles and more junk, *i.e.* disordered or amorphous particles (Figure 1C).

The variability between preparations suggested a fragile S ectodomain architecture. Indeed, fragility of the SARS-CoV-2 S ectodomain and measures to overcome its instability have been previously reported (*11, 13*). We traced the apparent spike fragility to rapid deterioration after storage at 4 °C (Figure 2 A-B), and hypothesized that the stabilized SARS-CoV-2 S ectodomain is a cold-sensitive protein. We tracked the behavior of the S ectodomain stored under different conditions using NSEM (Figure 2), SEC (Figure S1), thermostability measurements (Figures 3, S2) and binding studies (Figures 4, S3, S4).

NSEM results are summarized in Figure 2C. Freshly prepared spike samples showed 75% well-formed spikes on average. Spike fraction was slightly decreased to 64% by one cycle of freeze/thaw and to 59% by storage at room temperature for up to one week; whereas it was slightly increased to 83% by 1-week storage at 37 °C. Remarkably, storage at 4 °C caused a significant decrease to only 5% intact spike. We also found that well-formed spike could be recovered after cold-storage degradation with a 3-hour incubation at 37 °C (Figure 2C-D). Longer incubations at 37 °C yielded no further improvement (Figure 2C) and showed slight aggregation.

The S ectodomain was recently reported to exhibit conformational changes with pH (*13*), so we questioned whether the spike degradation we observed was due to the expected temperature-dependent pH change for Tris buffer (*14*). Therefore, we split a spike preparation and SEC-purified one fraction into Tris buffer pH 8.0, and the other into MOPS buffer pH 7.4, which is expected to change only slightly to pH 7.42 at 4 °C, due its smaller temperature dependence compared to Tris (*14*) . Room-temperature storage for one week at pH 8.0 (Tris

buffer) reduced the spike fraction to 50% (Figure 2C, green hatched bar), similar to the average of 59% after room-temperature storage. In contrast, cold-storage at pH 7.42 (MOPS buffer) reduced the spike fraction to 4% (Figure 2C, red hatched bar), similar to the average of 5% for cold-storage in Tris buffer. Thus, the primary cause of spike degradation here appears to be the temperature change and not the pH shift.

We next demonstrate that the observed cold-sensitivity is not merely an artifact of the negative stain sample preparation but is a property of the bulk protein in solution. First, we measured stability with DSF (*10*), and observed distinct profile shifts indicating lower stability when spike samples were stored at 4 °C (Figures 3 A-B). Next, we performed differential scanning calorimetry (DSC) on the spike samples to obtain quantitative measures of the melting temperatures, T_m (Figure 3 C-D and S2). After one week of storage at 37 °C, the spike sample demonstrated an asymmetric unfolding transition with a T_m of 65.5 °C. The observed peak was best fit with two Gaussian transition models (Figure S2) suggesting a complex unfolding mechanism. After sample storage at 22 °C for one week, we observed a second low-T_m transition at 48.2 °C. After sample storage at 4°C for one week, we observed a similar two-peak profile with a markedly more pronounced low-T_m transition (T_m = 48.4 °C). Upon returning the 4-°C sample to 37 °C for 3 hours prior to analysis, we observed an amplitude reduction of the low-T_m transition (T_m = 49.2 °C) and a corresponding amplitude increase in the high-T_m transition (T_m = 66.0 °C). The DSC results confirmed that storage at 4 °C destabilizes the spike compared to samples stored at 22 °C or 37 °C, and that returning the destabilized spike to 37 °C for 3 hours substantially restores its stability.

Because similar spike constructs are being widely used for vaccine studies including antibody and ligand binding, we next tested the effects of cold-induced instability on antibody and ligand binding by ELISA (Figures 4A-D; S3) and SPR (Figures 4 E-I, S3-S4). We found that

spike stored at 4 °C showed higher binding to ACE-2 and the RBD-directed antibody CR3022, both of which require an “up” RBD conformation (*2, 9, 13*). In contrast, cold storage reduced the binding by the antibody 2G12 (Figure 4D), which binds a quaternary glycan epitope in the S2 subunit (*15*), suggesting the quaternary epitope is disrupted by cold. We also tested two antibodies isolated from a COVID-19 convalescent patient (Figure 4 H-I, S3), one mapped to the ACE-2 binding site, AB712199 (Figures S3 A-B), and another mapped to the S2 region of the spike, AB511584 (Figure S3C). Consistent with its RBD-epitope, AB712199 binding levels were higher to the spike stored at 4 °C. AB511584 also showed increased levels of binding to the spike samples stored at 4 °C, suggesting it bound an S2 epitope that is better presented in the partially destabilized cold-stored S ectodomain.

Overall, our results demonstrate that storage temperature has a large effect on the stability of the SARS-CoV-2 ectodomain, with profound impact on its antigenic and binding properties. These results thus have direct impact on vaccine studies that rely on antigenic and binding measures for read-outs. Similar to our NSEM observations, we also see substantial differences in the quality and dispersion of protein in cryo-EM grids depending on how the specimen was stored (Figure S5). This is particularly relevant because optimal specimen preparation is crucial for obtaining high resolution cryo-EM data and 4 °C is often the default storage condition for most biochemists and structural biologists.

Our study raises two critical questions – first, how relevant are the observations made here to the biology of the native spike? And second, what implications do these results have for SASR-CoV-2 ectodomain vaccines? It remains to be seen if the results presented here translate to the biology of the native virion, and further experiments in a more native context will be needed to determine that. Nevertheless, the results presented here suggest a highly malleable internal architecture of the spike ectodomain consistent with its dynamic nature and our findings

that point at a fragile and temperature sensitive ectodomain have direct implications for vaccine studies.

Acknowledgements

This work was supported by NIH NIAID extramural project grants R01 AI145687 (P.A.), and AI058607 (G.S.), funding from the Department of Defense HR0011-17-2-0069 (G.S.) and a contract from the State of North Carolina Pandemic Recovery Office through funds from the Coronavirus Aid, Relief, and Economic Security (CARES) Act (B.F.H.). This work utilized the DSC platform supported by the Duke Consortia for HIV/AIDS Vaccine Development (CHAVD) and the Titan Krios microscope in the Shared Materials and Instrumentation Facility at Duke University.

Author contributions

R.J.E., K.Mansouri., V.S. and P.A. discovered the effect of storage temperature on spike stability. R.J.E. led NSEM studies and established quantitative metrics for spike QC. K.Mansouri collected NSEM data and performed analyses. V.S. purified proteins and performed thermostability measurements. K.Manne purified proteins, performed SPR assays, prepared samples for NSEM, Tycho, ELISA, SPR and DSC measurements, and coordinated the study between the different research teams. B.W. performed DSC measurements. R.P. and M.D. performed ELISA assays. D.L., X.L., K.S. and G.S. isolated antibodies from convalescent patient. S.G. and K. J. purified proteins and performed thermostability assays. W.W. performed ELISA assays. R.H. initiated the DSC experiments. M.A. supervised the DSC experiments. B.F.H. supervised ELISA experiments and antibody isolation. P.A. oversaw and led the study, and co-wrote the paper with R.J.E. and V.S. All authors reviewed and commented on the manuscript.

Methods

Protein expression and purification

SARS-CoV-2 ectodomain constructs were produced and purified (*2*) as follows. A gene encoding residues 1−1208 of the SARS-CoV-2 S (GenBank: MN908947) with proline substitutions at residues 986 and 987, a "GSAS" substitution at the furin cleavage site (residues 682–685), a C-terminal T4 fibritin trimerization motif, an HRV3C protease cleavage site, a TwinStrepTag and an 8XHisTag was synthesized and cloned into the mammalian expression vector pαH. Plasmids were transiently transfected into FreeStyle-293F cells using Turbo293 (SpeedBiosystems). Protein was purified on the sixth day post-transfection from filtered supernatant using StrepTactin resin (IBA), followed by SEC purification using a Superose 6 10/300 Increase column in nCoV buffer (2mM Tris, pH 8.0, 200 mM NaCl, 0.02% sodium azide).

Antibodies were produced in Expi293 cells and purified by Protein A affinity. For ACE-2 constructs, the ACE-2 C-terminus was fused with either the human or mouse Fc region including C-terminal 6X His-tag on the Fc domain. ACE-2 with human Fc tag was purified by Protein A affinity chromatography, and ACE-2 with mouse F_C tag was purified by Ni-NTA chromatography.

Negative-stain electron microscopy

Spike samples were pre-incubated (stored) for specified times in nCoV buffer at 4, 22 or 37 °C, then moved to room temperature for preparation of NSEM grids, which was complete in less than 5 min. Samples were diluted to 100 µg/ml with room-temperature buffer containing 20 mM HEPES pH 7.4, 150 mM NaCl, 5% glycerol and 7.5 mM glutaraldehyde, and incubated 5 min; then glutaraldehyde was quenched for 5 min by addition of 1M Tris stock to a final concentration of 75 mM. A 5-µl drop of sample was applied to a glow-discharged, carbon-coated grid for 10-15 s, blotted, stained with 2% uranyl formate, blotted and air-dried. Images were obtained with a

Philips EM420 electron microscope at 120 kV, 82,000× magnification, and a 4.02 Å pixel size. The RELION program (*16*) was used for particle picking and 2D class averaging.

Thermostability assays

Thermostability of the S ectodomain samples were measured using DSF and DSC. Samples were purified and buffer exchanged into HBS buffer (10 mM HEPES, 150 mM NaCl, pH 7.4) by SEC on a Superose 6 10/300 column. DSF assay was performed using Tycho NT. 6 (NanoTemper Technologies). Spike variants were diluted (0.15 mg/ml) in HBS and run in triplicate. Intrinsic fluorescence was recorded at 330 nm and 350 nm while heating the sample from 35–95 °C at a rate of 30 °C/min. The ratio of fluorescence (350/330 nm) and inflection temperatures (Ti) were calculated by Tycho NT. 6.

DSC measurements were performed using the NanoDSC platform (TA instruments; New Castle, DE) on samples freshly purified by SEC (Figure S1), diluted to 0.2–0.3 mg/mL in HBS, and degassed for 15 min at room temperature prior to analysis. DSC cells were conditioned with filtered, degassed HBS prior to sample loading. Protein samples were heated from 10 °C to 100 °C at 1 °C/min under 3 atm pressure using HBS as the reference buffer. The observed denaturation profiles were buffer subtracted, converted to molar heat capacity, baseline-corrected with a 6th-order polynomial, and fit with 2-4 Gaussian transition models, as needed, using the NanoAnalyze software (TA Instruments). The peak transition temperature (T_m) is reported as the temperature at the maximum observed heat capacity of each transition peak.

Isolation of antibodies from convalescent patients

Human SARS-CoV-2 Spike antibodies Ab712199 and Ab511584 were isolated from a COVID-19 convalescent individual. Briefly, PBMC samples collected after the onset of the symptoms were stained and the memory B cells were sorted with SARS-CoV-2 Spike-2p probes. Antibody

IgH and IgK/L genes were recovered from the single-cell sorted cells, cloned into human IgG1 constant region backbone, and purified by Protein A beads as previously described (*17*).

ELISA assays

Spike samples were pre-incubated at different temperatures then tested for antibody- or ACE-2-binding in ELISA assays as previously described (*18, 19*). Assays were run in two formats. In the first format antibodies or ACE-2 protein were coated on 384-well plates at 2 µg/ml overnight at 4°C, washed, blocked and followed by two-fold serially diluted spike protein starting at 25 µg/ml. Binding was detected with polyclonal anti-SARS-CoV-2 spike rabbit serum (developed in our lab), followed by goat anti-rabbit-HRP (Abcam #ab97080) and TMB substrate (Sera Care Life Sciences #5120-0083). Absorbance was read at 450 nm. In the second format, serially diluted spike protein was bound in individual wells of 384-well plates, which were previously coated with streptavidin (Thermo Fisher Scientific #S-888) at 2 µg/ml and blocked. Proteins were incubated and washed, then human mAbs were added at 10 µg/ml. Antibodies were incubated, washed and binding detected with goat anti-human-HRP (Jackson ImmunoResearch Laboratories, #109-035-098) and TMB substrate.

Commercially obtained constructs of SARS-CoV-2 spike ectodomain (S1+S2 ECD, S2 ECD and RBD) (Sino Biological Inc cat# 40589-V08B1 and 40590-V08B respectively and RBD from Genescript cat# Z03483) were coated directly on 384-well plates at 2 µg/ml and incubated overnight at 4 °C. Plates were washed, blocked and human mAbs three-fold serially diluted from 100 µg/ml were added for 1 h at room temp followed by washing. Binding was detected with Goat anti-human IgG-HRP followed by TMB substrate.

Surface Plasmon Resonance

Antibody binding to SARS-CoV-2 spike constructs was assessed by surface plasmon resonance on a Biacore T-200 (GE-Healthcare) at 25°C with HBS buffer with 3 mM EDTA and

0.05% surfactant P-20 added. Antibodies captured on a CM5 chip coated with amine-coupled human Anti-Fc (8000RU) were assayed by SARS-CoV-2 spike at 200 nM. The surface was regenerated between injections with 3 M $MgCl_2$ solution for 10 s at 100 µl/min. Sensorgram data were analyzed using the BiaEvaluation software (GE Healthcare).

Cryo-EM

Purified SARS-CoV-2 spike preparations were diluted to a concentration of ~1 mg/mL in 2 mM Tris pH 8.0, 200 mM NaCl and 0.02% NaN_3. A 2.5-µL drop of protein was deposited on a CF-1.2/1.3 grid that had been glow discharged for 30 seconds in a PELCO easiGlow™ Glow Discharge Cleaning System. After a 30 s incubation in >95% humidity, excess protein was blotted away for 2.5 seconds before being plunge frozen into liquid ethane using a Leica EM GP2 plunge freezer (Leica Microsystems). Frozen grids were imaged in a Titan Krios (Thermo Fisher) equipped with a K3 detector (Gatan).

References

1. Z. Ke, Oton, J.; Qu, K.; Cortese, M.; Zila, V.; McKeane, L.; Nakane, T.; Zivanov, J.; Neufeldt, C.J.; Lu, J.M.; Peukes, J.; Xiong, X.; Krausslich, H.G.; Scheres, S.H.W.; Bartenschlager, R.; Briggs, J.A.G., Structures, conformations and distributions of SARS-CoV-2 spike protein trimers on intact virions. *bioRxiv*, (2020).
2. D. Wrapp *et al.*, Cryo-EM structure of the 2019-nCoV spike in the prefusion conformation. *Science* **367**, 1260-1263 (2020).
3. A. C. Walls *et al.*, Structure, Function, and Antigenicity of the SARS-CoV-2 Spike Glycoprotein. *Cell* **181**, 281-292 e286 (2020).
4. C. O. Barnes *et al.*, Structures of human antibodies bound to SARS-CoV-2 spike reveal common epitopes and recurrent features of antibodies. *bioRxiv*, (2020).
5. D. Pinto *et al.*, Cross-neutralization of SARS-CoV-2 by a human monoclonal SARS-CoV antibody. *Nature*, (2020).
6. C. E. Mire *et al.*, A Cross-Reactive Humanized Monoclonal Antibody Targeting Fusion Glycoprotein Function Protects Ferrets Against Lethal Nipah Virus and Hendra Virus Infection. *J Infect Dis* **221**, S471-S479 (2020).
7. L. Liu *et al.*, Potent Neutralizing Monoclonal Antibodies Directed to Multiple Epitopes on the SARS-CoV-2 Spike. *bioRxiv*, (2020).
8. T. Zhou *et al.*, Structure-Based Design with Tag-Based Purification and In-Process Biotinylation Enable Streamlined Development of SARS-CoV-2 Spike Molecular Probes. *bioRxiv*, (2020).
9. R. Henderson *et al.*, Controlling the SARS-CoV-2 Spike Glycoprotein Conformation. *bioRxiv*, (2020).
10. A. O. Magnusson *et al.*, nanoDSF as screening tool for enzyme libraries and biotechnology development. *FEBS J* **286**, 184-204 (2019).
11. C. L. Hsieh *et al.*, Structure-based Design of Prefusion-stabilized SARS-CoV-2 Spikes. *bioRxiv*, (2020).
12. R. Henderson *et al.*, Glycans on the SARS-CoV-2 Spike Control the Receptor Binding Domain Conformation. *bioRxiv*, (2020).
13. T. Zhou *et al.*, A pH-dependent switch mediates conformational masking of SARS-CoV-2 spike. *bioRxiv*, (2020).
14. N. E. Good *et al.*, Hydrogen ion buffers for biological research. *Biochemistry* **5**, 467-477 (1966).
15. P. Acharya *et al.*, A glycan cluster on the SARS-CoV-2 spike ectodomain is recognized by Fab-dimerized glycan-reactive antibodies. *bioRxiv*, (2020).
16. S. H. W. Scheres, in *Methods in Enzymology,* R. A. Crowther, Ed. (Academic Press, 2016), vol. 579, pp. 125-157.
17. H. X. Liao *et al.*, Co-evolution of a broadly neutralizing HIV-1 antibody and founder virus. *Nature* **496**, 469-476 (2013).
18. S. M. Alam *et al.*, Mimicry of an HIV broadly neutralizing antibody epitope with a synthetic glycopeptide. *Science translational medicine* **9**, (2017).
19. M. Bonsignori *et al.*, Staged induction of HIV-1 glycan-dependent broadly neutralizing antibodies. *Science translational medicine* **9**, (2017).

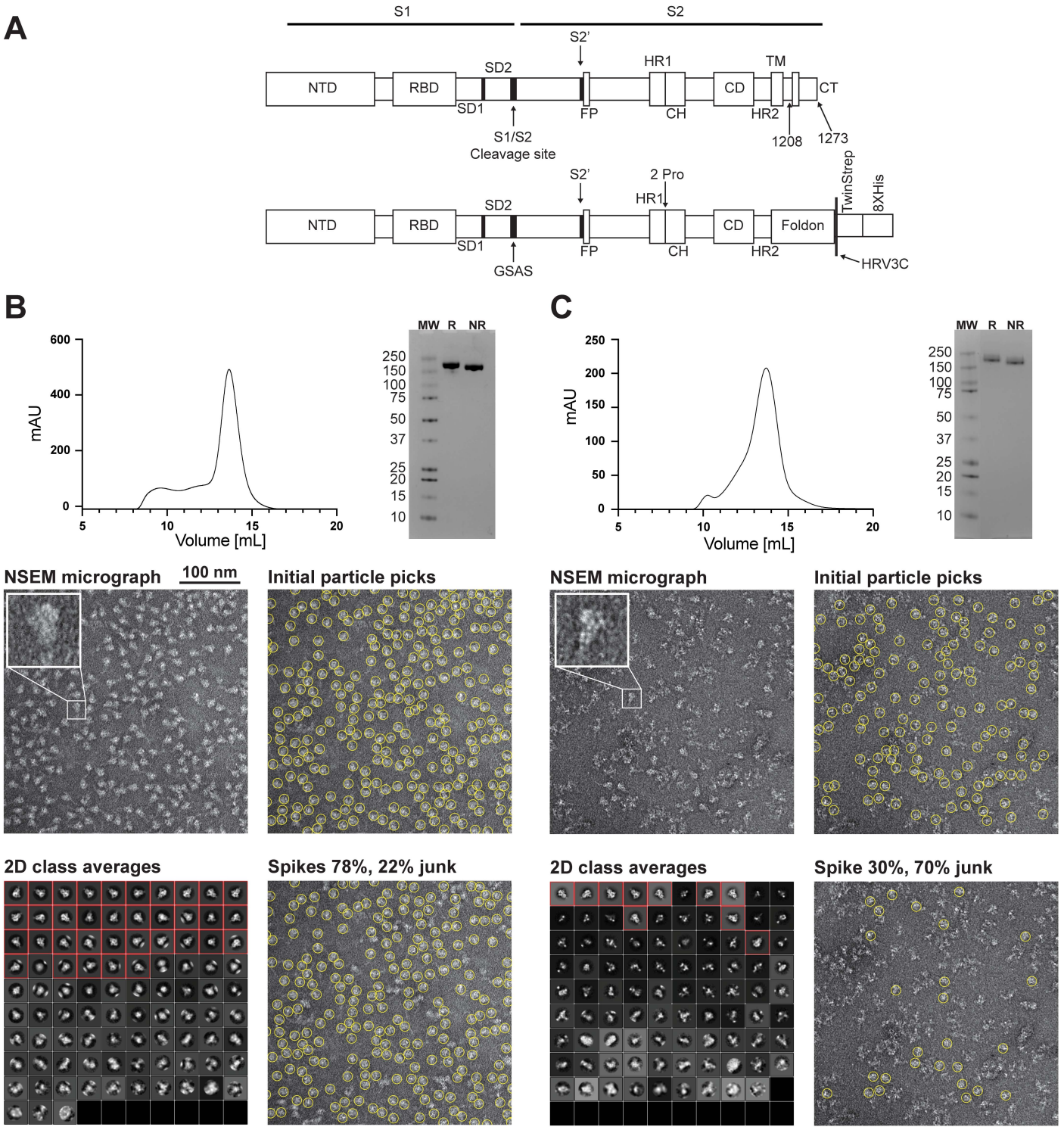
A
S1
S2
S2'
SD2
HR1
TM
NTD
RBD
CD
CT
SD1
FP
CH
HR2
S1/S2
Cleavage site
1208
1273
S2'
2 Pro
HR1
TwinStrep
8XHis
SD2
NTD
RBD
CD
Foldon
SD1
FP
CH
HR2
GSAS
HRV3C
B
mAU
Volume [mL]
MW R NR
C
mAU
Volume [mL]
MW R NR
NSEM micrograph
100 nm
Initial particle picks
2D class averages
Spikes 78%, 22% junk
NSEM micrograph
Initial particle picks
2D class averages
Spike 30%, 70% junk

Figure 1. Purification and quality control of the SARS-CoV-2 S protein ectodomain for vaccine studies. (A) Schematic of the SARS-CoV-2 spike (top) and a stabilized ectodomain construct (bottom). The furin cleavage site between the S1 and S2 subunits is mutated making the construct cleavage-deficient, and two proline mutations engineered in the S2 domain stabilize the construct (2). **(C and D)** Two representative spike preparations that together highlight the role of NSEM in discriminating between good **(C)** and bad **(D)** spike preparations that otherwise appear to be of similar quality by SEC (top, left) and SDS-PAGE (top, right). Representative micrographs from each prep are shown, middle left. Protein appears as white blobs on gray background. Insets show a single kite-shaped spike particle enlarged. At the middle right, automatic particle picking is shown as yellow circles superimposed on the micrograph. Sets of ~20,000 initial particles picks are subjected to automated 2D classification to group together and average particles with similar features into discrete classes, bottom left. In the 2D class averages for each sample, the classes that contain the SARS-Cov-2 S ectodomain (shown within red boxes) can be clearly distinguished from classes that contain junk. The final spike picks come from the particles contained within the indicated classes and their total number provide an estimate of the ratio between the SARS-CoV-2 S ectodomain and junk seen in the NSEM sample.

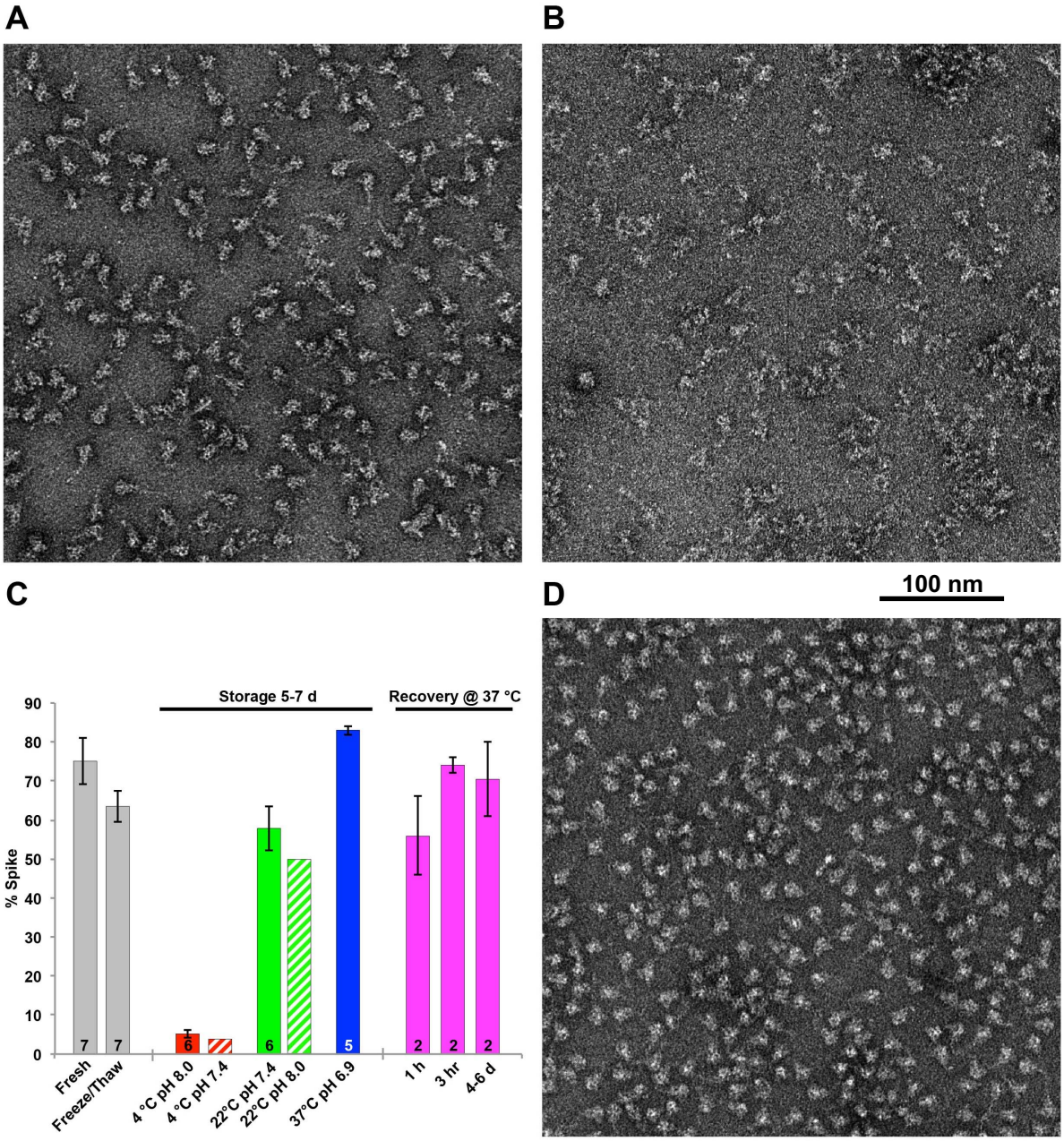

Figure 2. Temperature-dependence of the SARS-CoV-2 S ectodomain. (A) Representative NSEM micrograph from a freshly prepared sample of the SARS-CoV-2P S ectodomain construct. **(B)** NSEM sample prepared after storing the same protein batch in A for one week at 4 °C. **(C)** Bar graph summarizing results from NSEM on SARS-CoV-2 S ectodomain samples that were stored under different conditions. From left to right, bars show spike percentage in a fresh sample of spike; after the spike undergoes a single freeze-thaw cycle; after it has been incubated for 5-7 says at 4 °C (red), 22 °C (green) or 37 °C (blue); and spike samples that were stored for 1 week at 4 °C, then incubated at 37 °C for 1 hour, 3 hours, or 4-6 days. Solid bars indicate averages, with error bars indicating standard error of the mean and the number of samples indicated at the bottom of each column. Hatched bars represent measurements from a single sample. **(D)** NSEM sample after storing the same protein batch in A for one week at 4 °C followed by a 3-hour incubation at 37 °C.

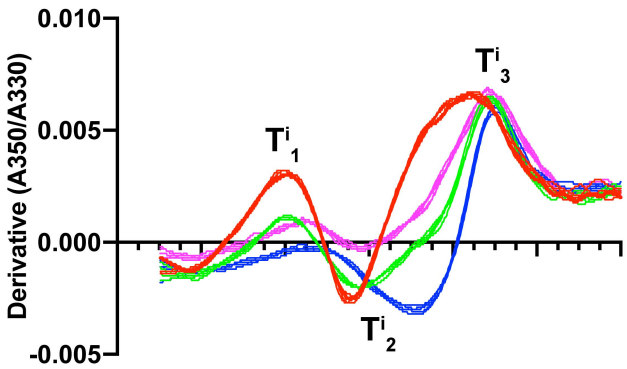

B

Storage Temperature	T^i_1	T^i_2	T^i_3
37 °C	53.7 ± 1.1	65 ± 0.2	74.8 ± 0.2
22 °C	49.9 ± 0.2	58.6 ± 0.3	74.2 ± 0.2
4 °C	49.9 ± 0.4	57.5 ± 0.3	71.9 ± 0.2
4->37 °C Recovery	52.2 ± 0.5	58.8 ± 0.5	74.1 ± 0.3

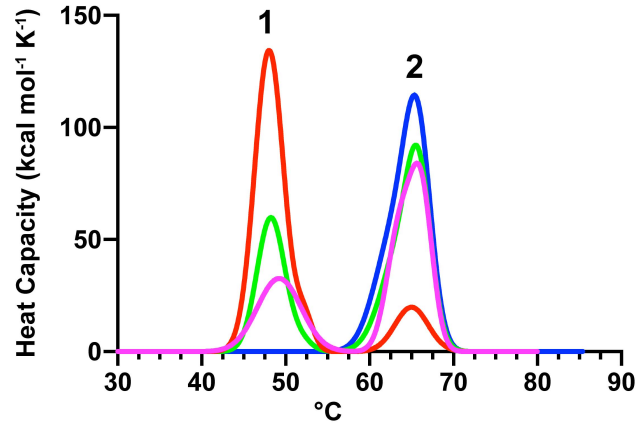

D

Storage Temperature	Transition Peak 1 T_m (°C)	Transition Peak 2 T_m (°C)
37 °C	N/A	65.5 ± 0.1
22 °C	48.23 ± 0.04	65.8 ± 0.1
4 °C	48.41 ± 0.01	65.1 ± 0.2
4->37 °C Recovery	49.21 ± 0.05	65.95 ± 0.01

Figure 3. Thermostability of SARS-CoV-2 spike ectodomain samples incubated at different temperatures. (A) Differential scanning fluorimetry profiles obtained by following changes in intrinsic fluorescence upon applying a thermal ramp to the sample and expressed as the first derivative of the ratio between fluorescence at 350 nm and 330 nm. Maxima and minima indicate inflection temperatures, T^i. Unfolding data for spike samples measured after a 1-week incubation at 37, 22, and 4 °C, are shown with blue, green, and red lines respectively; sample stored 1 week at 4 °C and then incubated for 3 hours at 37 °C shown with magenta lines. Horizontal axis same as in C. **(B)** Table of inflection temperatures, expressed as averages ± standard deviation, N=5. Storage at 4 °C lowers T^i values compared to storage at 37 °C, indicating protein instability after cold storage. Values after storage at 22 °C, or 37-°C-recovery after cold storage are intermediate. **(C)** Thermal denaturation profiles obtained by differential scanning calorimetry indicate two discrete transition peaks, a high-Tm transition (~65 °C) and a low-Tm transition (~48 °C), the proportions of which are dependent on sample storage conditions. **(D)** Table of melting temperatures, T_m, with values expressed as averages ± standard deviation, N=2

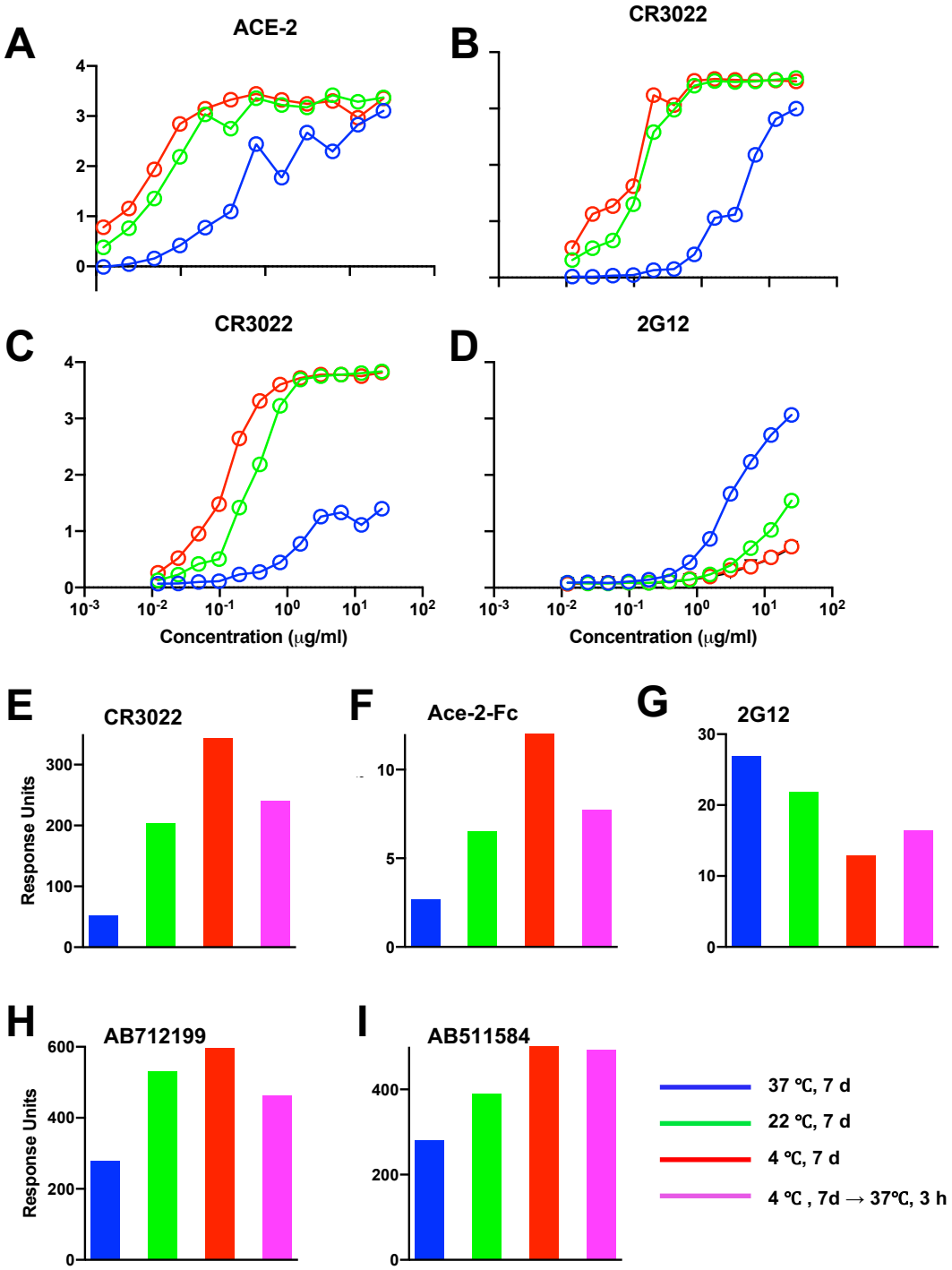

Figure 4. Antigenicity of SARS-CoV-2 S ectodomain samples after incubation at different temperatures. (A) Binding of ACE-2 and **(B)** CR3022 to spike incubated at different temperatures. **(A,B)** ACE-2 with a mouse Fc tag and CR3022 IgG were coated on the ELISA plate, and titrated with different concentrations of the spike that were incubated for 1 week at either 37 °C (blue), 22 °C (green) or 4 °C (red) **(C)** Binding of CR3022 and **(D)** 2G12 to spike. **(C,D)** ELISA plate was coated with streptavidin. Different concentrations of spike was captured on the plate and detected with 10 μg/ml of antibody. **(E-I)** Antibody or ligand-binding of spike stored at different temperatures as measured by SPR. **(E)** CR3022 IgG, **(F)** ACE-2-Fc, **(G)** 2G12 IgG, and with two antibodies that were isolated from convalescent patient serum, **(H)** AB712199 and **(I)** AB511584. SPR profiles shown in Figures S3-4.

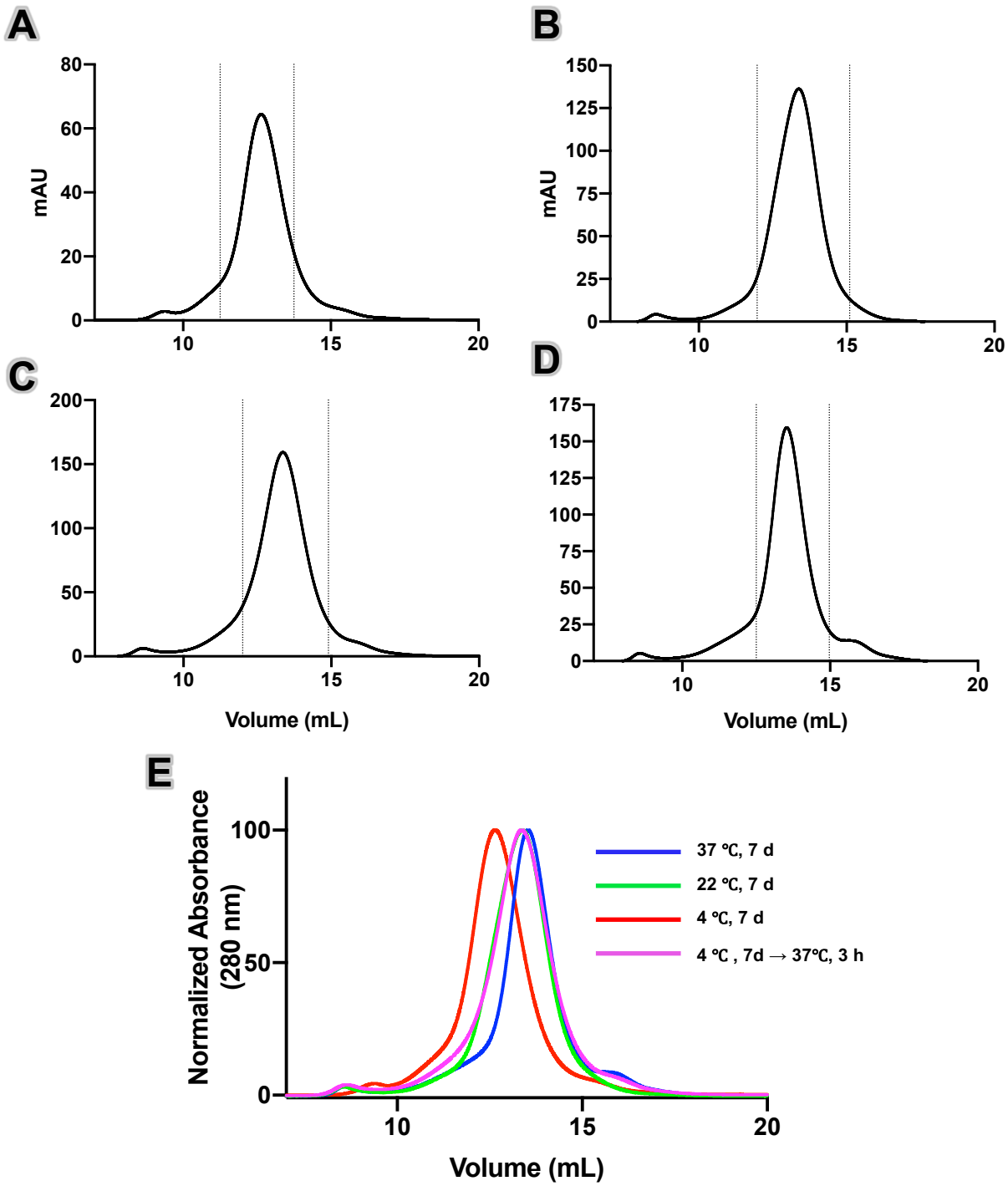

Figure S1. Size Exclusion Chromatography of SARS-CoV-2 S ectodomain incubated at different temperatures. SEC profiles run on a Superose 6 increase 10/300 column for SARS-CoV-2 S ectodomain samples that were incubated at **(A)** 4 °C for one week, **(B)** 22 °C for one week. **(C)** 37 °C for one week, and **(D)** 4 °C for one week and moved to 37 °C for 3 hours prior to the experiment. **(E)** Overlay of SEC plots normalized to allow better visualization of peak shifts.

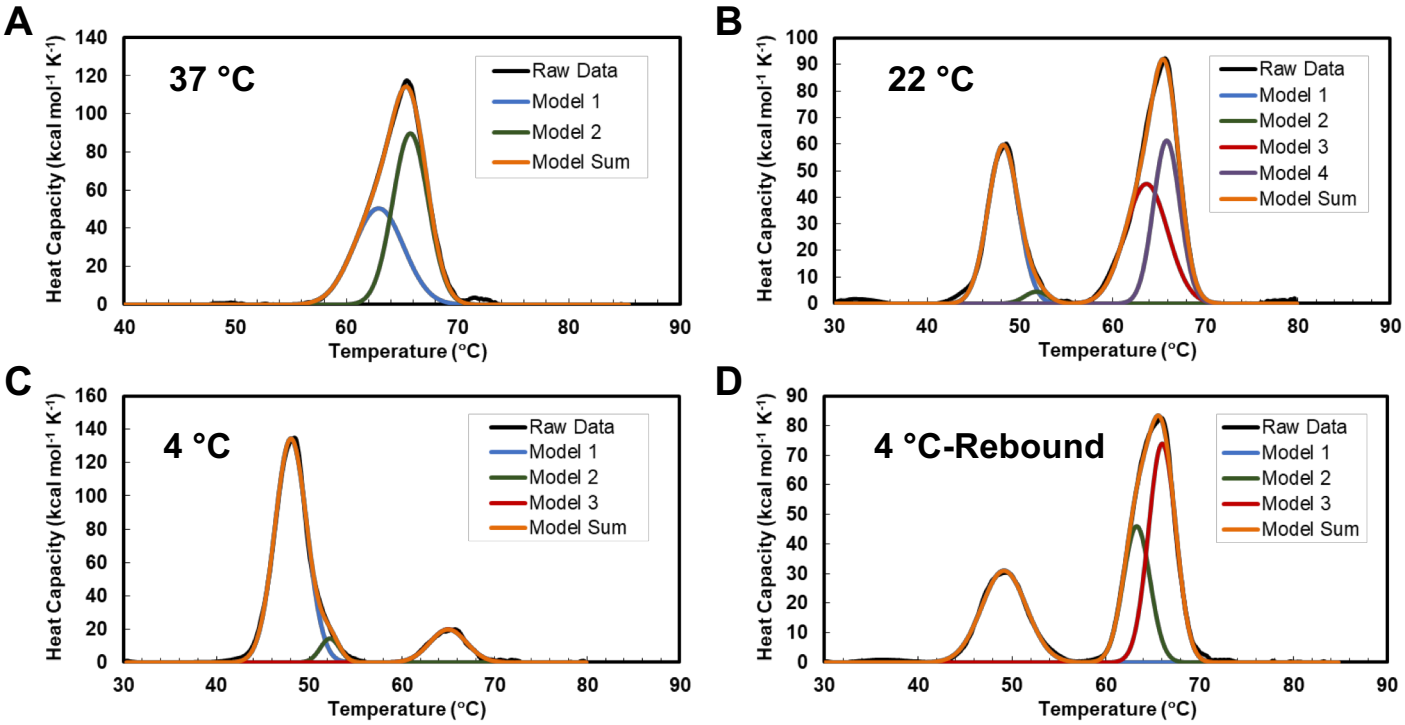

E

	Transition Peak 1		Transition Peak 2		DSC Model Fits			
	T_{onset} (°C)	T_m (°C)	T_{onset} (°C)	T_m (°C)	$T_{m,1}$ (°C)	$T_{m,2}$ (°C)	$T_{m,3}$ (°C)	$T_{m,4}$ (°C)
37 °C	N/A	**N/A**	57.5 ± 0.3	**65.5 ± 0.1**	63.2 ± 0.5	65.74 ± 0.01	N/A	N/A
22 °C	43.64 ± 0.01	**48.23 ± 0.04**	58.5 ± 0.9	**65.8 ± 0.1**	48.23 ± 0.04	51.9 ± 0.02	63.5 ± 0.3	65.92 ± 0.04
4 °C	43.0 ± 0.3	**48.41 ± 0.01**	61.1 ± 0.1	**65.1 ± 0.2**	48.02 ± 0.02	52.4 ± 0.2	65.1 ± 0.2	N/A
4 °C-Rebound	42.5 ± 0.4	**49.21 ± 0.05**	59.59 ± 0.03	**65.95 ± 0.01**	49.21 ± 0.05	63.4 ± 0.2	66.1 ± 0.1	N/A

Figure S2. Thermostability of the SARS-CoV-2 spike ectodomain stored at different temperatures. Representative thermal denaturation profiles of the SARS-CoV-2 spike ectodomain after 1 week incubations at (**A**) 37 °C , (**B**) 22 °C, (**C**) 4 °C, and (**D**) 4 °C followed by 37 °C for 3 hours. Profiles and transition parameters (**E**) were obtained by DSC and analyzed as described in Methods. Raw data (black) was best fit with two or more Gaussian transition models ($T_{m,1\text{-}4}$) (blue, green, red, purple). Data shown are the mean and standard deviation from two replicate measurements.

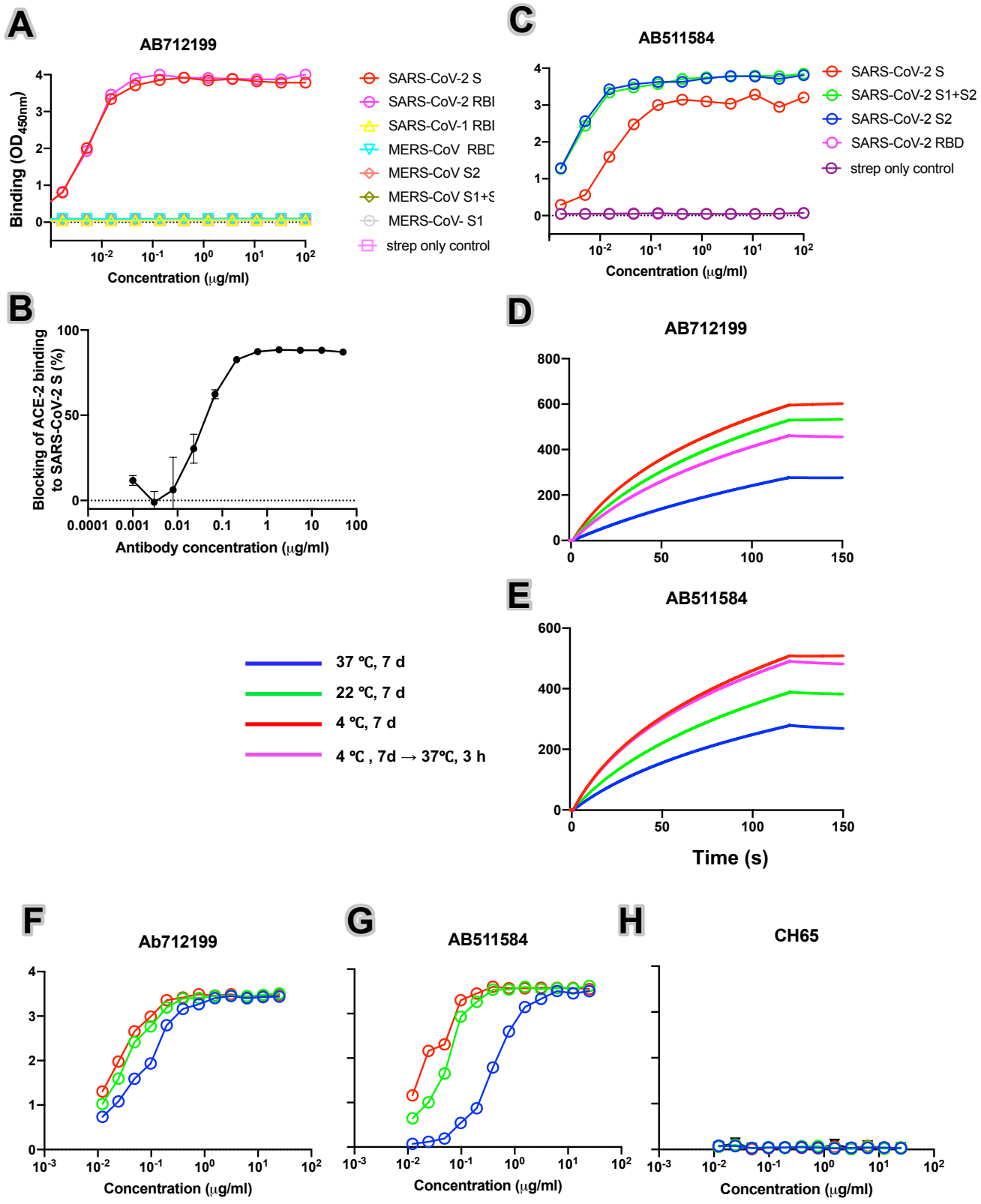
A
AB712199
Binding (OD450nm)
Concentration (μg/ml)
SARS-CoV-2 S
SARS-CoV-2 RBI
SARS-CoV-1 RBI
MERS-CoV RBD
MERS-CoV S2
MERS-CoV S1+S
MERS-CoV- S1
strep only control
C
AB511584
SARS-CoV-2 S
SARS-CoV-2 S1+S2
SARS-CoV-2 S2
SARS-CoV-2 RBD
strep only control
Concentration (μg/ml)
B
Blocking of ACE-2 binding to SARS-CoV-2 S (%)
Antibody concentration (μg/ml)
D
AB712199
E
AB511584
Time (s)
37 ℃, 7 d
22 ℃, 7 d
4 ℃, 7 d
4 ℃ , 7d → 37℃, 3 h
F
Ab712199
G
AB511584
H
CH65
Concentration (μg/ml)

Figure S3. Antigenic response of SARS-CoV-2 S ectodomain incubated at different temperatures to antibodies elicited from convalescent patient sera. (**A**) Epitope mapping of AB712199 isolated from convalescent patient #26 that shows that the antibody binds the SARS-CoV-2 RBD region, (**B**) Blocking of ACE-2 binding to SARS-CoV-2 S ectodomain by AB712199, **(C)** Epitope mapping of AB511584 isolated from convalescent patient #26 that shows that the antibody binds the SARS-CoV-2 S2 region (**D-E**) SPR binding profiles showing binding of **(D)** RBD-directed antibody, AB712199, **(E)** S2-directed antibody, AB511584 to spike samples incubated for 1 week at either 37 °C (blue), 22 °C (green) or 4 °C (red). Binding to spike sample first incubated at 4 °C for 1 week, then moved to 37 °C for 3 hours prior to the experiment is shown in magenta. **(F-H)** ELISA binding profiles showing binding of **(F)** RBD-directed antibody, AB712199, **(G)** (middle) S2-directed antibody, AB511584, or **(H)** influenza HA-directed antibody CH65 (control) to spike samples incubated for 1 week at either 37 °C (blue), 22 °C (green) or 4 °C (red).

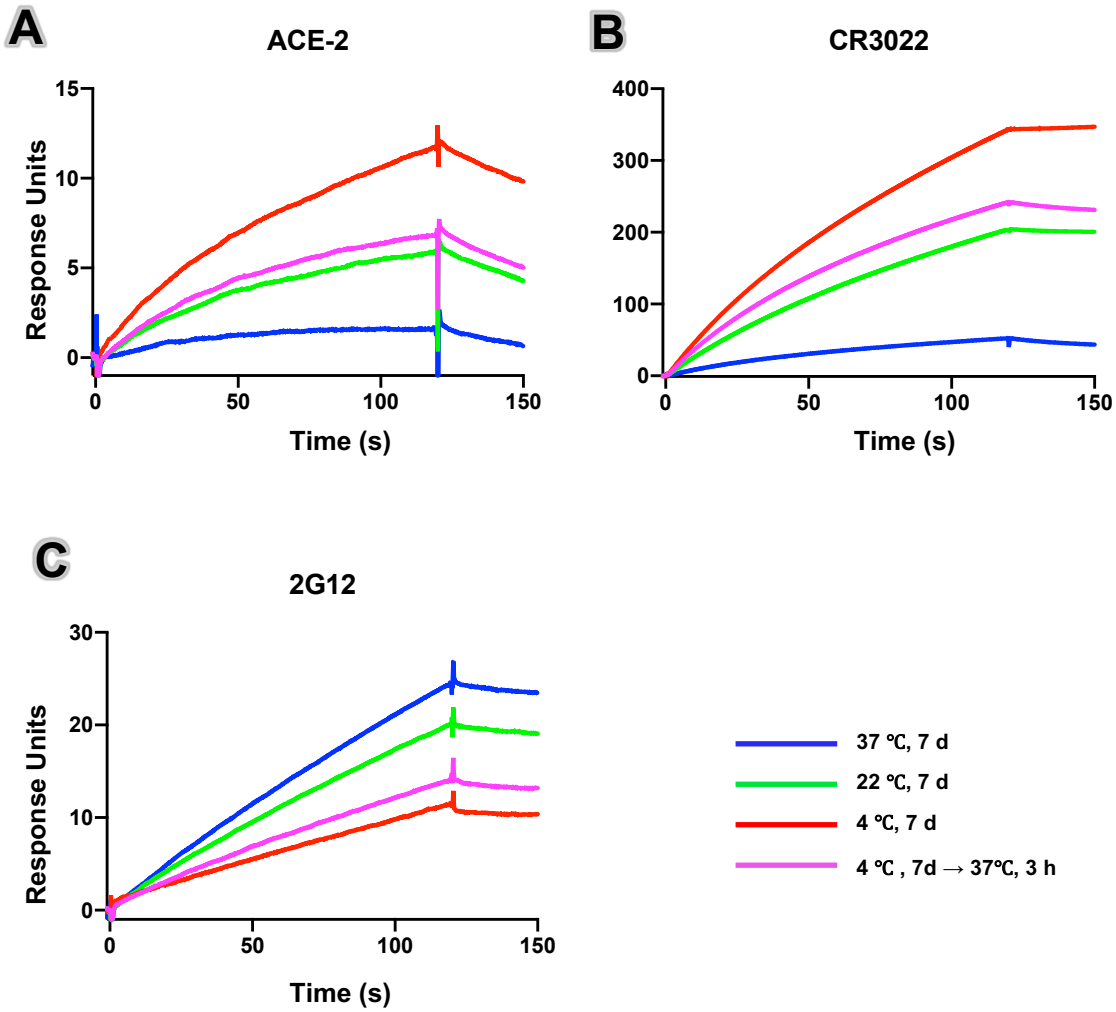

Figure S4. Changes in antigenicity of SARS-CoV-2 S ectodomain incubated at different temperatures. SPR profiles showing binding of **(A)** ACE-2, **(B)** RBD-directed antibody, CR3022, and **(C)** S2 glycan-directed antibody 2G12 to spike samples incubated for 1 week at either 37 °C (blue), 22 °C (green) or 4 °C (red). Binding to spike sample first incubated at 4 °C for 1 week, then moved to 37 °C for 3 hours prior to the experiment is shown in magenta

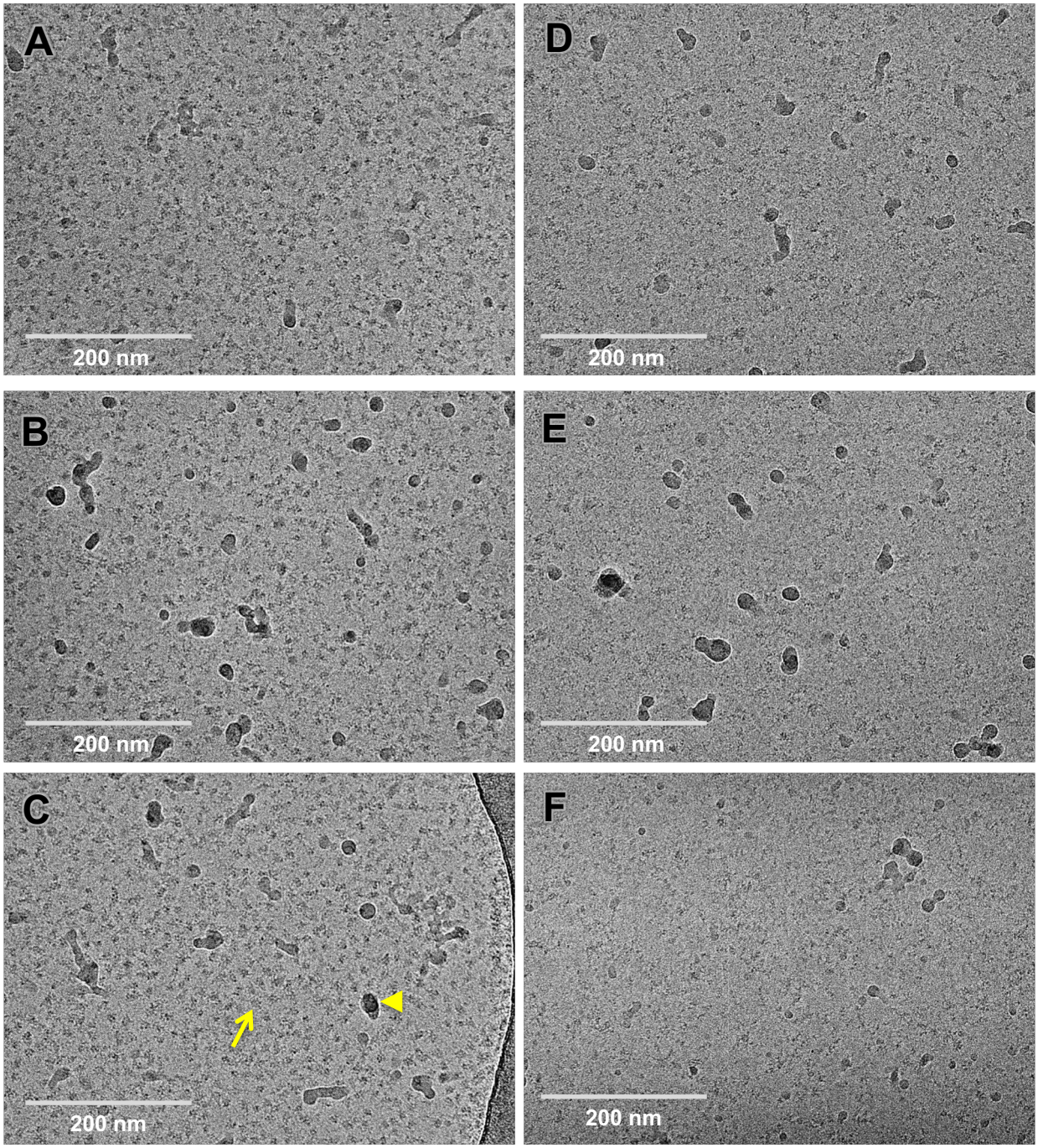

Figure S5. Effect of SARS-CoV-2 ectodomain spike sample storage on cryo-EM specimen preparation. (**A-C**) Representative cryo-EM micrographs of a SARS-CoV-2 S ectodomain sample that was flash frozen immediately after purification and stored in -80 °C, then thawed rapidly and incubated for ~ 5 min at 37 °C immediately prior to grid preparation. Cryo-EM images are low contrast, and the desired spike particles appear as medium gray spots (*e.g.* arrow) on a light gray background. Dark gray or black spots are slight ice contamination (*e.g* arrowhead). These panels on the left show an excellent distribution of discrete spike particles. **(D-F)** Representative cryo-EM micrographs of SARS-CoV-2 S ectodomain samples that were stored for ~1 week at 4 °C prior to grid preparation. Compared to the panels of the left, these panels on the right show a sparse field-of-view with very few intact spike particles visible. A similar spike concentration (~1 mg/ml) was used to freeze all the samples. Micrographs were collected on a Titan Krios microscope with a Gatan K3 camera.